Materials Chemistry and Physics 284 (2022) 126030

Contents lists available at ScienceDirect

Materials Chemistry and Physics

journal homepage: www.elsevier.com/locate/matchemphys

The spin effects on electronic, optical and mechanical properties of new ferromagnetic chalcopyrite: $YMnS_2$

Bugra Yildiz [a,*], Aytac Erkisi [b], Gokhan Surucu [c,d]

[a] Hacettepe University, Department of Physics Engineering, Ankara, 06800, Turkey
[b] Pamukkale University, Department of Physics, Denizli, 20020, Turkey
[c] Department of Electric and Energy, Ahi Evran University, Kirsehir, 40100, Turkey
[d] Middle East Technical University, Department of Physics, Ankara, 06800, Turkey

HIGHLIGHTS

- Ferromagnetic phase is most suitable for this compound.
- It is understood from the electronic band structure of $YMnS_2$ compound has half-metallic nature.
- The material could be good candidate for optoelectronic applications.
- Determined elastic constants indicate that the material has high incompressibility and ductility.
- The estimated low thermal conductivity show that it could be a good candidate for thermal barrier coating applications.

ARTICLE INFO

Keywords:
Half-metallic
Mechanical
Optical and electronic properties
Density functional theory

ABSTRACT

In this study, magnetic and electronic nature, optical behavior, and elasticity properties of $YMnS_2$ compound have been investigated by using density functional theory (DFT). The compound belongs to the chalcopyrite family having tetragonal crystal structure with 122 (*I-42d*) space group. Firstly, the optimization process has been done for ferromagnetic, antiferromagnetic, and paramagnetic orders to find most stable magnetic order and the formation energies have been determined. Negative formation energies prove that our compound is energetically synthesizable and structurally stable. For this compound, plotted energy change with respect to volume curves show that ferromagnetic order is most stable. It is understood from the electronic band structure obtained with Perdew-Burke-Ernzerhof functional within Generalized Graident Approximation, which has 1.27 eV band gap for spin-up orientation and metallic for spin-down orientation, so overall $YMnS_2$ compound has a half-metallic nature. Moreover, the electronic band structure has been obtained with HSE06 functionals that indicates the half-metallic nature with 3.20 eV band gap in spin-up orientation and metallic nature in spin-down orientation. To understand optical properties, frequency dependent complex dielectric functions have been determined. Then, some optical properties have been investigated using the imaginary and real parts of the dielectric function. In addition to that, $YMnS_2$ compound is mechanically stable according to Born-Huang stability criteria. Also, this new chalcopyrite compound is considered to be ductile, which is important for its use in technological applications.

1. Introduction

Semiconductor or half-metallic chalcopyrite structures have been very popular for many years, since they have been used in several applications such as thermoelectric [1–3], magnetism [4,5], photovoltaic cells [6], optical devices [7], spintronics (i.e. spin-dependent electronic devices), giant magneto-resistance, and the magnetic sensors [8,9]. Moreover, half-metallic materials can also show metallic or semiconducting behavior due to their spin state. And they can produce electrical conduction, resulting from the charge carriers of a particular spin direction only. In addition, they have 100% spin-polarization, and it generates spin-polarized current. This feature yields the optimum

* Corresponding author.
E-mail address: bugrayildiz@hacettepe.edu.tr (B. Yildiz).

https://doi.org/10.1016/j.matchemphys.2022.126030
Received 13 September 2021; Received in revised form 26 February 2022; Accepted 20 March 2022
Available online 22 March 2022

efficiency for magnetoelectronic devices. It could be stated that half-metallic materials also have magneto-optical properties. Moreover, they can be candidate for many applications, like electrical switches where only one type of electrons. These properties make half-metallics suitable for spin-dependent electronic and magneto-optical devices [10,11].

$CuFeS_2$ is the prototype of chalcopyrites and it is theoretically and experimentally most studied structure among this family with 122 *(I-42d)* space group. In the literature, the physical properties of $CuFeS_2$ under doping were examined and the temperature dependence of the Seebeck coefficient were investigated. Also, it has been shown that the most stable magnetic phase of $CuFeS_2$ is the antiferromagnetic phase [12–18]. In addition, electronic structure, and Boltzmann transport theory calculations for $CuFeS_2$ were studied with Density Functional Theory (DFT) [19]. Moreover, figure of merit ZT, lattice thermal conductivity, and the total and projected densities of states were obtained theoretically, and these results were confirmed experimentally [20–22].

$AgFeS_2$ is another widely studied compound in this family which is known as lenaite. The first study on the physical properties of this compound was carried out by J. W. Boon in 1944. Then, the formation energy of this compound was calculated, and its magnetic and opto-electronic properties were investigated. In addition, optical and mechanical properties of $AgFeS_2$ were extensively studied [23–25].

The ductile or the brittle nature of a material is another important feature for the industrial applications. The ductile materials absorb relatively higher energy and undergo less plastic deformation, and it makes them preferable in the industry. To get the ductile material from the chalcopyrite family, Cu/Ag could be replaced with Y [26,27].

The motivation to search a new material which has both half metallic nature and the ductile property guided us to study $YMnS_2$ structure belonging to chalcopyrite family.

In this work, $YMnS_2$ compound has been investigated using Density Functional Theory (DFT) in detail for the first time in terms of its structural, magnetic, electronic, optical, and mechanical properties.

2. Computational details

In this research, Density Functional Theory (DFT) calculations have been done using Vienna Ab Initio Simulation Package (VASP) [28–30]. The optimization procedure has been continued iteratively until all the pressures and the forces on each atom become zero. This process has been performed in order to determine the most appropriate magnetic order among ferromagnetic, antiferromagnetic, and paramagnetic orders with the formation energies. Then, the electronic band structure with the density of states have been calculated and plotted for the most stable magnetic phase that is determined as ferromagnetic. Furthermore, some optical properties of the related material have been investigated with the calculated complex dielectric function.

Perdew-Burke-Ernzerhof (PBE) [31] type exchange and correlation functionals have been considered within Generalized Gradient Approximations (GGA). For *Y*, *Mn* and *S* atoms, the valance electron configurations are $4s^2 4p^6 5s^2 4d^1$, $3p^6 3d^5 4s^2$ and $3s^2 3p^4$, respectively. 6 × 6 × 8 MP (Monkhorst-Pack) k-point mesh has been used for sampling reciprocal space [32]. The cut off energy has been chosen as 500 eV. Also, the projector augmented wave (PAW) method has been employed to describe interaction between electrons and ion cores. Methfessel-Paxton type smearing method has been used in which smearing parameter has chosen as 0.01 eV. The positions of atoms in the cell have been fixed until the minimum force on atoms reach 10^{-10} eV/Å. Furthermore, the hybrid functional Heyd-Scuseria-Ernzerhof (HSE) method [33] has been employed to prevent the underestimation of the band gaps of semiconductors resulted from the GGA-PBE method. For the HSE method, the screened HSE06 hybrid functional is taken with the screening parameter of 0.2 $Å^{-1}$ and 25% of the exact non-local Hartree-Fock exchange which is mixed into the exchange part [34]. The elastic constants have been calculated with the "stress–strain" approximation as implemented in VASP using IBRION = 6 and ISIF = 3 parameters [35]. Some elastic properties such as bulk and shear modules have been obtained by ELATE program [36].

3. Results and discussion

3.1. The structural properties

$YMnS_2$ compound belongs to the chalcopyrite family with 122 (*I-42d*) space group [37] is given in Fig. 1. To construct the unit cell of $YMnS_2$, the chalcopyrite structure was chosen as a prototype [38]. $YMnS_2$ compounds in which two Y atoms are placed at 4a (0, 0, 0), two Mn atoms are positioned on 4b (0.5, 0.5, 0) and finally four S atoms are located at 8d (0.161, 0.125, 0.250) Wyckoff positions.

In Fig. 1, three-dimensional (3D) crystallographic structure and X-Ray diffraction pattern (XRD) obtained with the optimization of the theoretical data have been illustrated. XRD pattern shows that the maximum 2θ value has been determined as 26.67° corresponding to the preferred orientation along the [112] direction. In addition, the obtained minor peaks around $2\theta = 44.10°$ and $2\theta = 52.71°$ correspond to the [203] and [133] directions, respectively. Since there are no results on the XRD studies for $YMnS_2$ compound, the obtained orientations within the present study could light the way to future studies.

The formation energy (ΔE_f), that could be determined by internal energies and total energy [39] as given in Eq. (1), is a vital parameter to understand thermodynamic and structural stability of a compound. For the formation energy calculation, the ground state energy of $YMnS_2$ and the ground state energies of one Y, one Mn and one S atoms are needed. E_{atom}^{bulk} is the ground state energy of one atom which is obtained in its bulk form.

$$\Delta E_f = E_{YMnS_2}^{bulk} - \left(E_Y^{bulk} + E_{Mn}^{bulk} + 2E_S^{bulk}\right) \quad (1)$$

where, E_{Total}^{bulk} symbolize total energy of the unit cell of the crystalline. Moreover, E_Y^{bulk}, E_{Mn}^{bulk} and E_S^{bulk} are the calculated ground state energies of *Y*, *Mn* and *S* atoms in their bulk crystals, respectively.

To examine the spin effects on $YMnS_2$, ferromagnetic, antiferromagnetic, and paramagnetic orders have been considered. For the ferromagnetic order, magnetic moments of the atoms aligned in the same direction. On the other hand, for the antiferromagnetic order, arrangement of the magnetic moments for the Mn atoms were oriented in antiparallel direction to yield zero magnetization and finally for the paramagnetic order all the magnetic moments of the atoms were given zero [40].

The calculated formation energies of the $YMnS_2$ compound for all three of magnetic orders along with lattice parameters and bond lengths have been tabulated in Table 1. The lattice parameters (a and c) and bond lengths (d) have been given for the most stable magnetic phase. After that, in order to clearly detect the most favorable magnetic phase, the energy-volume plot has been drawn for the considered three types of magnetic orders given as in Fig. 2. The ground state energy values have been normalized by using Vinet equations [41]. The plotted energy-volume curves and the calculated formation energies show that for this chalcopyrite, the ferromagnetic phase is the most stable, since it has the lowest ground state energy in Fig. 2. In addition to that, as one can see from Table 1, negative formation energies prove that $YMnS_2$ compound is energetically synthesizable and structurally stable. Also, in ferromagnetic order, it has lowest bond lengths. In addition, although $YMnS_2$ compound has same crystal structure with other chalcopyrite and lenaite compounds, lattice parameter c is relatively smaller than the others as listed in Table 1. This result is due to the larger atomic radii of Y and Mn atoms than Ag, Cu and Fe atoms.

The total magnetic moment of a compound which has ferromagnetic behavior, is an important parameter to better understand its magnetic nature. In this view, the partial magnetic moments (in μ_B) of each atom and the total magnetic moment (in μ_B) of this chalcopyrite have been

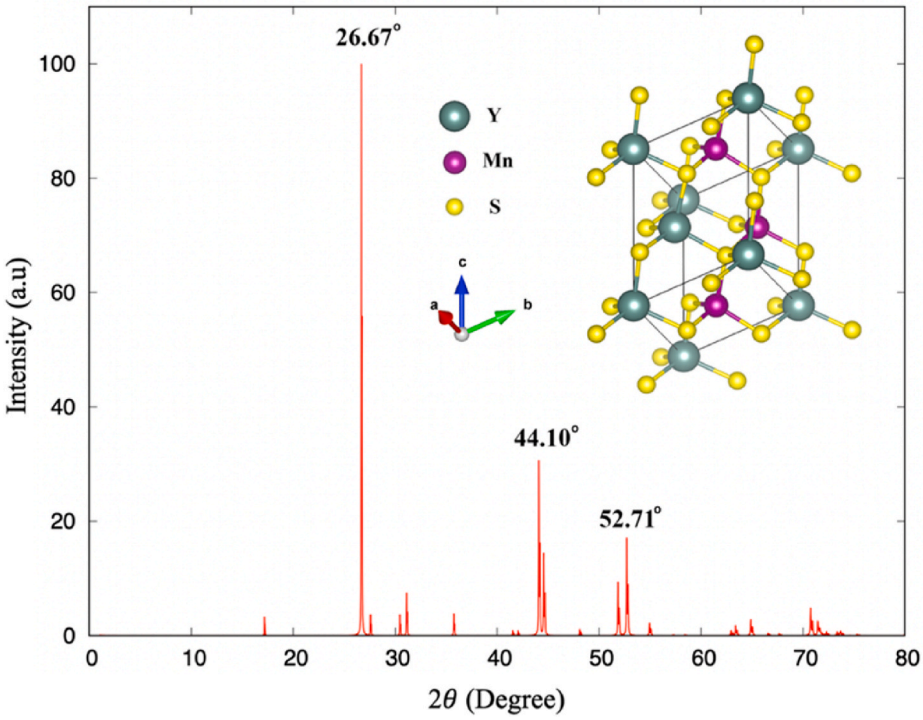

Fig. 1. The three-dimensional crystallographic structure and X-Ray diffraction pattern (XRD) of $YMnS_2$. Where a.u is arbitrary unit.

Table 1
The lattice parameters (a and c) and bond lengths (d) given in Å. The calculated formation energies (ΔE_f) given in $eV/f.u$ for three different type of magnetic orders.

Compounds	*A*	*c*	$d_{Mn,\ Fe-S}$	$d_{Y,Cu-S}$	ΔE_f
$YMnS_2$	5.740	7.154	2.393 (FM)	2.627 (FM)	−4.391 (*FM*)
			2.513 (AFM)	2.759 (AFM)	−4.193 (*AFM*)
			2.513 (PM)	2.759 (PM)	−2.979 (*PM*)
$AgFeS_2$ [25]	5.637	10.240			
$CuFeS_2$ [42]	5.289	10.423	2.257	2.302	

Table 2
The computed total and partial magnetic moments (μ_B) of $YMnS_2$.

Compounds	μ_Y	μ_{Mn}	μ_S	μ_{Total}	
$YMnS_2$	−0.093	3.691	0.064	3.660	
$AgFeS_2$ [25]				GGA	3.091
				(GGA + U)+SOC	3.535
				GGA + U	3.536
$CuFeS_2$ [16]				3.8	

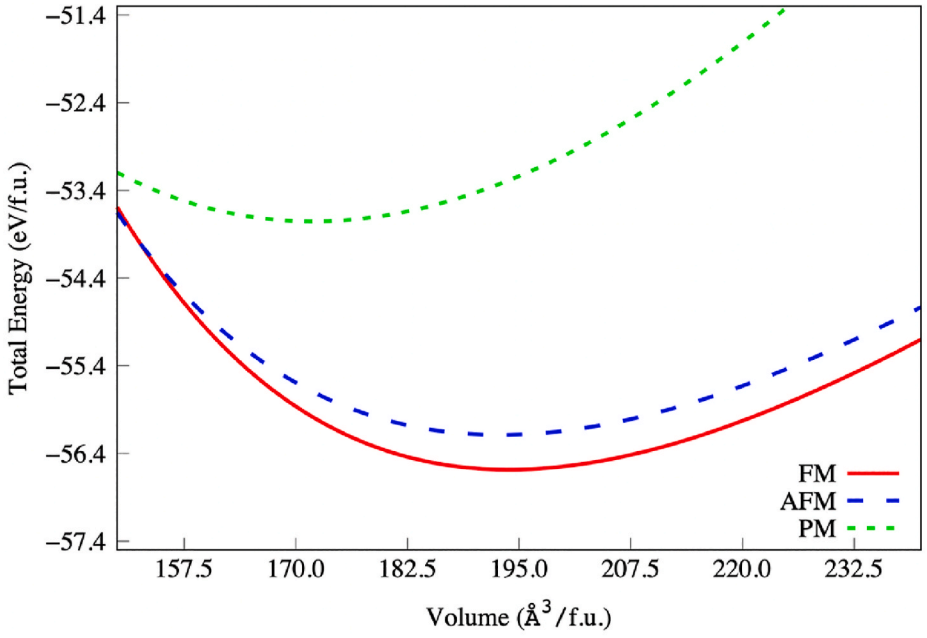

Fig. 2. The energy-volume curves of $YMnS_2$ for ferromagnetic, antiferromagnetic and paramagnetic orders.

computed and presented in Table 2. It is clear from this table that the greatest contribution to the total magnetic moment comes from the Mn atom. Also, total magnetic moment of $YMnS_2$ is lower than $CuFeS_2$ and higher than $AgFeS_2$ compound as listed in Table 2.

3.2. Electronic properties

In this part of the study, to discover the electronic behavior of this chalcopyrite, its electronic band structure under spin-polarization have been investigated using the PBE and HSE06 functionals. Also, for the ferromagnetic phase which is the most stable magnetic order for this compound, the orbital projected total density of states (TDOS) and partial density of states of atoms (PDOS) have been calculated. The observed electronic band structure in the first Brillouin zone along the high symmetry points is given in Fig. 3 obtained with PBE functional (shown in black) and HSE06 functional (shown in red). Also, for both spin-up and spin-down orientations, the detailed partial density of states of each atom in the mentioned composition are given in Fig. 4 obtained with PBE and HSE06 functionals. As can be seen from Fig. 3., the observed electronic band structure indicates 1.27 eV indirect band gap obtained with PBE functional and 3.20 eV indirect band gap obtained with HSE06 functional for the spin-up channel while the spin-down channel has no gap as in calculations with both functionals. That means our compound has half-metallic nature with both PBE and HSE06 functionals. The band gap obtained with the HSE06 functional in the spin-up channel is higher than that is obtained with PBE functional consistent with the well-known underestimation of the PBE functional. From Fig. 4., the dominant effect to the total density of states comes from the *d*- orbital of *Mn* atoms and *d*- orbital of *Y* atoms while *S* atoms contribution to the partial density of states is lower than the *Y* and *Mn* atoms for both functionals. For spin-down orientation, it is clearly seen that hybridization of d-orbital of *Y* and *Mn* atoms around Fermi energy level causes metallic property in this orientation. In this regard, the half-metallic behavior and bonding characteristic of this compound are determined mainly by the *d*-orbitals of the manganese (*Mn*) and yttrium (*Y*) atoms, and the hybridizations between them around Fermi level. Furthermore, the Bader partial charges have been calculated using VASP and determined using Bader charge analysis program [43]. The total Bader charges are 2.47, 1.15, and −3.62 for Y, Mn and S atoms, respectively. The positive charge for Y and Mn atoms indicates the charge transferred away from the atoms whereas the negative charge for S atoms indicates the charge transfer to the atom.

3.3. Optical properties

Density functional theory has been successfully applied to investigate the optical properties of $YMnS_2$ compound. To understand the optical properties of the related compound, it is vital to determine both imaginary and real part of dielectric function. The dielectric function could be determined by using the eigenvectors which are founded by using corresponding Schrödinger equation. The dielectric function is given by [44,45] Eq. (2);

$$\varepsilon(\omega) = \varepsilon^{real}(\omega) + i\varepsilon^{imag}(\omega) \tag{2}$$

Both real and imaginary parts of dielectric function are given in Fig. 5a as a function of photon energy. In addition to that, the real and imaginary parts of dielectric function could be used to calculate other important optical parameters such as refractive index ($n(\omega)$), extinction coefficient ($\kappa(\omega)$), loss function ($L(\omega)$) and absorption ($I(\omega)$) coefficient [46]. The obtained optical properties as a function of photon energy are given in Fig. 5.

The real part of dielectric function is related to electronic polarization and imaginary part of dielectric function is related to ability to absorb light [47]. As one can deduct from Fig. 5a that both imaginary and real parts of dielectric function have greater value below visible region. Also, the negative value of real part between 8 eV and 14 eV indicates that the material has metallic characteristic [48]. Moreover, the imaginary part illustrates that there is a sharp rise at low energy, which is due to indirect intra-band excitations that this compound exhibits a metallic character.

The value at the zero frequency $\varepsilon(0)$ is crucial as the electronic part of the static dielectric function. However, the ionic contribution should be added to the electronic contribution to get the static dielectric function. Fig. 6 shows the ionic contribution to the complex dielectric function. The static field contribution of the ionic lattice to the dielectric constant was calculated as $\varepsilon_\infty = 37.7129$, $\varepsilon_{ion} = 1.15937$ and $\varepsilon_o(=\varepsilon_\infty+\varepsilon_{ion}) =$

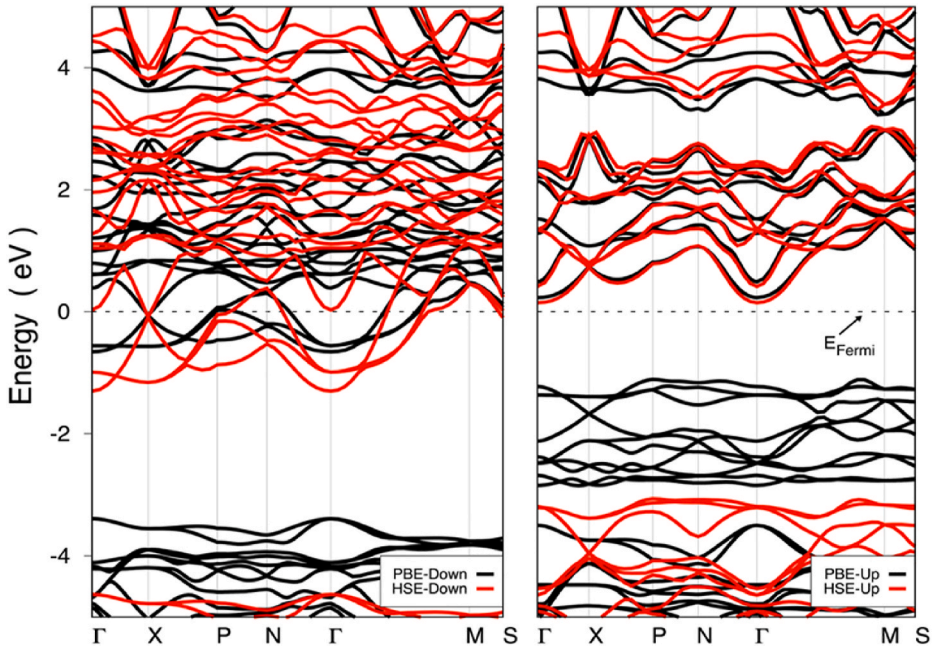

Fig. 3. The calculated band structures for spin-down orientation (left) and spin-up orientation (right) of $YMnS_2$ using PBE (black lines) and HSE06 (red lines) functional. The black dashed line represents the Fermi level, which is set to zero. (For interpretation of the references to colour in this figure legend, the reader is referred to the Web version of this article.)

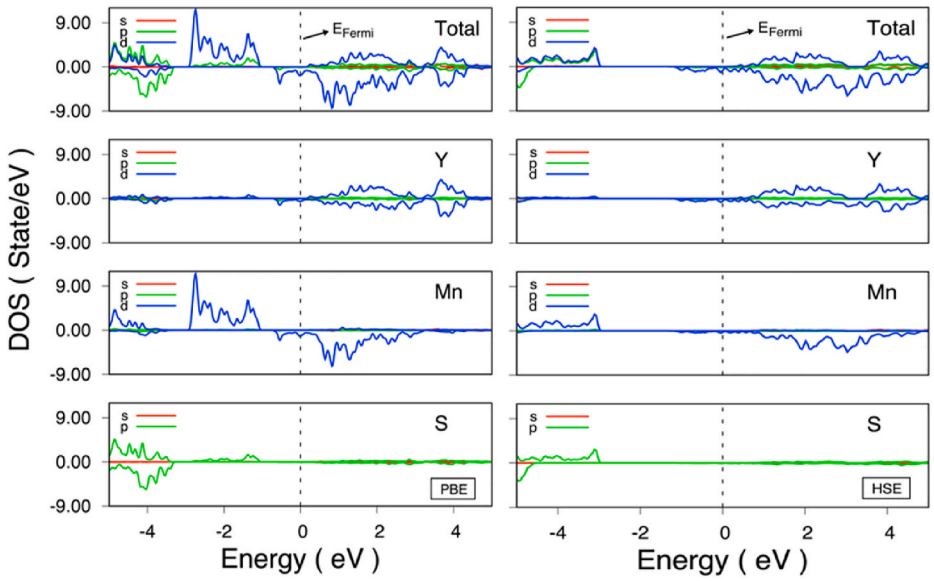

Fig. 4. The DOS (density of states) for the atoms in $YMnS_2$ compound calculated by PBE (left) and HSE06 (right) functionals.

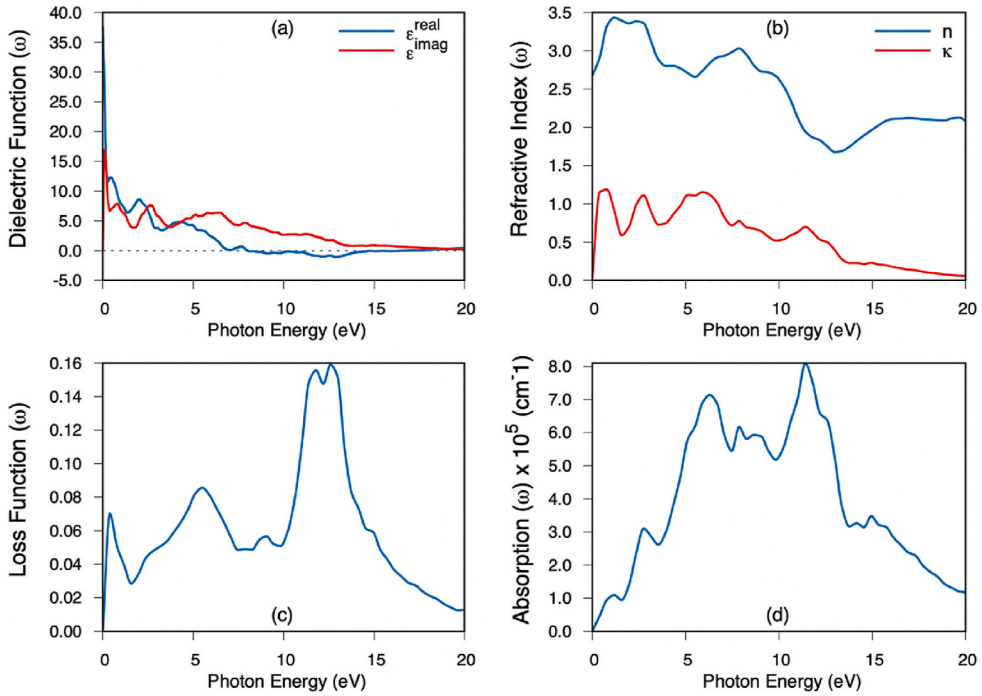

Fig. 5. The (a) dielectric function ($\varepsilon(\omega)$), (b) refractive index ($n(\omega)$) and extinction index ($\kappa(\omega)$) (c) loss function ($L(\omega)$) and (d) absorption ($I(\omega)$) as a function of photon energy for $YMnS_2$ material.

38.87227. In addition, ion-clamped dielectric constant was obtained in the frequency range between 50 and 60 Hz.

Absorption capability of the incident photon which has a specific frequency can be determined from the computed absorption coefficient I (ω). Moreover, this parameter points out the suitability of a material's band gap and its absorption for optoelectronic and photovoltaic applications [49]. In this regard, this chalcopyrite compound could be good candidate for photovoltaic applications due to their high absorption in the visible region and the band gap in spin-up orientation of the calculated electronic band structure. Refractive index which is given in Fig. 5b, starts from 2.70 and reach its maximum value around visible region (1.0–3.0 eV) as 3.46. While refractive index has minimum value around 13 eV, loss and absorption function reaching their maximum value around this energy in Fig. 5c and d.

3.4. Elastic properties

To determine the mechanical stability and the durability to the against external forces of $YMnS_2$ compound, all the elastic constants (C_{ij}) have been calculated. It is well known that, there are six independent elastic constants for any tetragonal crystal system [50] and for this study, the calculated constants have been tabulated in Table 3. In order to determine mechanical stability of $YMnS_2$ compound, Born-Huang stability criteria [51] have been checked according to inequality

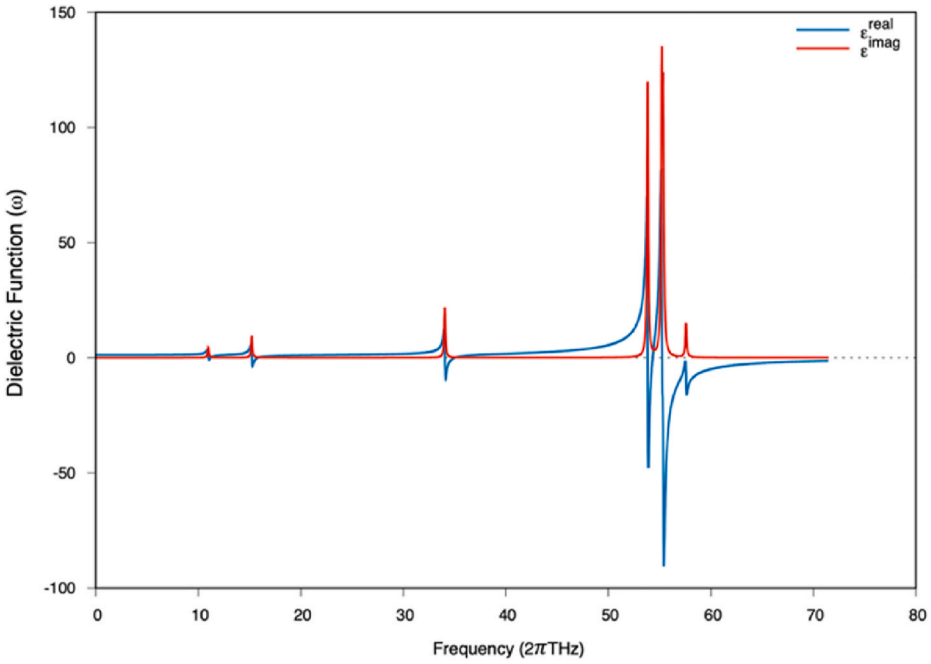

Fig. 6. The ionic contribution to the complex dielectric function.

Table 3
The determined elastic constants (C_{ij}) in GPa, for $YMnS_2$ compound.

Compound	C_{11}	C_{33}	C_{44}	C_{66}	C_{12}	C_{13}
$YMnS_2$	69.4	74.4	10.2	9.2	50.7	53.1
$AgFeS_2$ [25]	82.9	68.4	51.6	55.0	57.5	52.7

equations are given in Eq. (3). In this regard, it can be said that $YMnS_2$ compound is mechanically stable. $C_{ii} > 0 C_{11} - C_{12} > 0$

$$C_{11} + C_{33} - 2C_{13} > 0$$

$$2C_{11} + C_{33} + 2C_{12} + 4C_{13} > 0 for \;\; i = 1,\ 3,\ 4,\ 6 \tag{3}$$

In order to be used in various engineering fields for any compound, it is very important to estimate its elastic properties. Firstly, shear (G) and bulk moduli (B), which are among the mechanical properties, were estimated using elastic constants. To predict the lower, upper limits and the average value of these moduli, Reuss [52], Voigt [53] and Hill [54] approximations have been used, respectively. The equations required to calculate the mentioned moduli of a tetragonal crystal are given explicitly in Eqs. (4)–(8) [55].

$$B_V = (1/9)[2(C_{11} + C_{12}) + C_{33} + 4C_{13}] \tag{4}$$

$$B_R = \left[(C_{11} + C_{12})C_{33} - 2C_{13}^2\right]^2 \Big/ \left[(C_{11} + C_{12}) + 2C_{33} - 4C_{13}\right] \tag{5}$$

$$G_V = (1/30)[(C_{11} + C_{12}) + 2C_{33} - 4C_{13} + 3C_{11} - 3C_{12} + 12C_{44} + 6C_{66}] \tag{6}$$

$$G_R = 15 \Big/ \left[\frac{18B_V}{\left[(C_{11} + C_{12})C_{33} - 2C_{13}^2\right]^2} + \frac{6}{C_{11} - C_{12}} + \frac{6}{C_{44}} + \frac{3}{C_{66}}\right] \tag{7}$$

$$(B_H = (B_V + B_R)/2 and (G_H = (G_V + G_R)/2 \tag{8}$$

Other features such as Pugh's (B/G) and Poisson's (ν) ratios or Young's (E) modulus could be estimated by using bulk and shear modulus calculated previously. To predict these parameters, Eqs. (9) and (10) could be used [55]. The values of the predicted parameters have been tabulated in Table 4.

$$\nu = \frac{3B - 2G}{2(3B + G)} \tag{9}$$

$$E = \frac{9BG}{3B + G} \tag{10}$$

The ductility or brittleness of any material can be deduced from Pugh's ratio as the ratio of bulk modulus to shear modulus (B/G). It is known that when the Pugh's ratio is higher than 1.75 [56], the ductility of the material tends to increase. The calculated Pugh's ratio indicates that this material has high ductility. The compressibility of any material can be understood from the value of Poisson's ratio (ν). If the Poisson's ratio reaches 0.5, the compound can be considered as incompressible material [57] and its value is also 0.25 for ionic bonds and 0.1 for covalent bonds [58]. As given in Table 4, this value is around 0.422. Therefore, it is understood that incompressibility of our material is high and also, bonding type of this system is nearly ionic.

It could be deduced from Tables 3 and 4 that $YMnS_2$ compound has lower elastic constants, bulk, shear and Young's moduli than $AgFeS_2$ compound. Although $YMnS_2$ has similar electronic and optical properties with other chalcopyrite compounds, ductility of this material is higher. Additionally, the shear anisotropy factors for {001} and {100} planes have been calculated with the help of Eq. (11) and Eq. (12) [59]. The estimated shear anisotropy factors for, $A_{\{100\}}$ and $A_{\{001\}}$ are 1.085

Table 4
The predicted mechanical properties of $YMnS_2$. B stands for bulk modulus (in *GPa*) whereas G stands for shear modulus (in *GPa*). B/G is Pugh's ratio, E is Young's modulus (in *GPa*) and finally ν stands for Poisson's ratio.

Compound	B_V	B_R	B_H	G_V	G_R	G_H	B/G	E	ν
$YMnS_2$	58.56	58.35	58.45	9.65	9.63	9.64	6.08	27.41	0.422
$AgFeS_2$ [25]	62.21	60.97	61.59	36.38	21.95	29.17	–	75.57	–

and 0.984, respectively. The calculated shear anisotropy factors for {001} and {100} planes are different from the unity that indicates the anisotropic nature of $YMnS_2$ compound.

$$A_{\{001\}} = \frac{4C_{66}}{(C_{11} - C_{12})} \tag{11}$$

$$A_{\{100\}} = \frac{4C_{44}}{(C_{11} + C_{33} - 2C_{13})} \tag{12}$$

To do a further investigation, the direction dependent two- and three-dimensional presentations of Young's modulus, linear compressibility, shear modulus and Poisson's ratio have been drawn by using ELATE software [36] as shown in Fig. 7. The blue and green lines, which are maximum and minimum values, are very close to each other and have spherical symmetry. In addition, Fig. 7 indicates that Young's modulus, Shear modulus and Poisson's ratio for $YMnS_2$ compound are isotropic in the (yz) plane while linear compressibility is isotropic in (xy) plane. On the other hand, all these properties are anisotropic in the other planes.

The wave velocities could be obtained from Navier's equations [60] which are given in Eqs. (13)–(15). The longitudinal (v_l), transverse (v_t), average wave velocities (v_m) have been calculated as 4467, 1640 and 1862 m/s respectively and the Debye temperature (Θ_D) have been obtained from these values as 191.7 K. Debye temperature is vital parameter to understand thermal behavior of a compound. Greater Debye temperature could mean higher melting temperature and thermal conductivity. To estimate minimum value of the thermal conductivity of this system, two different model which are Cahill [61] and Clarke model [62], have been used. The estimated values for the minimum thermal conductivity are 0.516 and 0.397 $Wm^{-1}K^{-1}$, which are relatively low and the materials with low thermal conductivity may be used in thermal barrier coating applications [63].

$$v_l = \left(\frac{B}{\rho} + \frac{4G}{3\rho}\right)^{\frac{1}{2}} \tag{13}$$

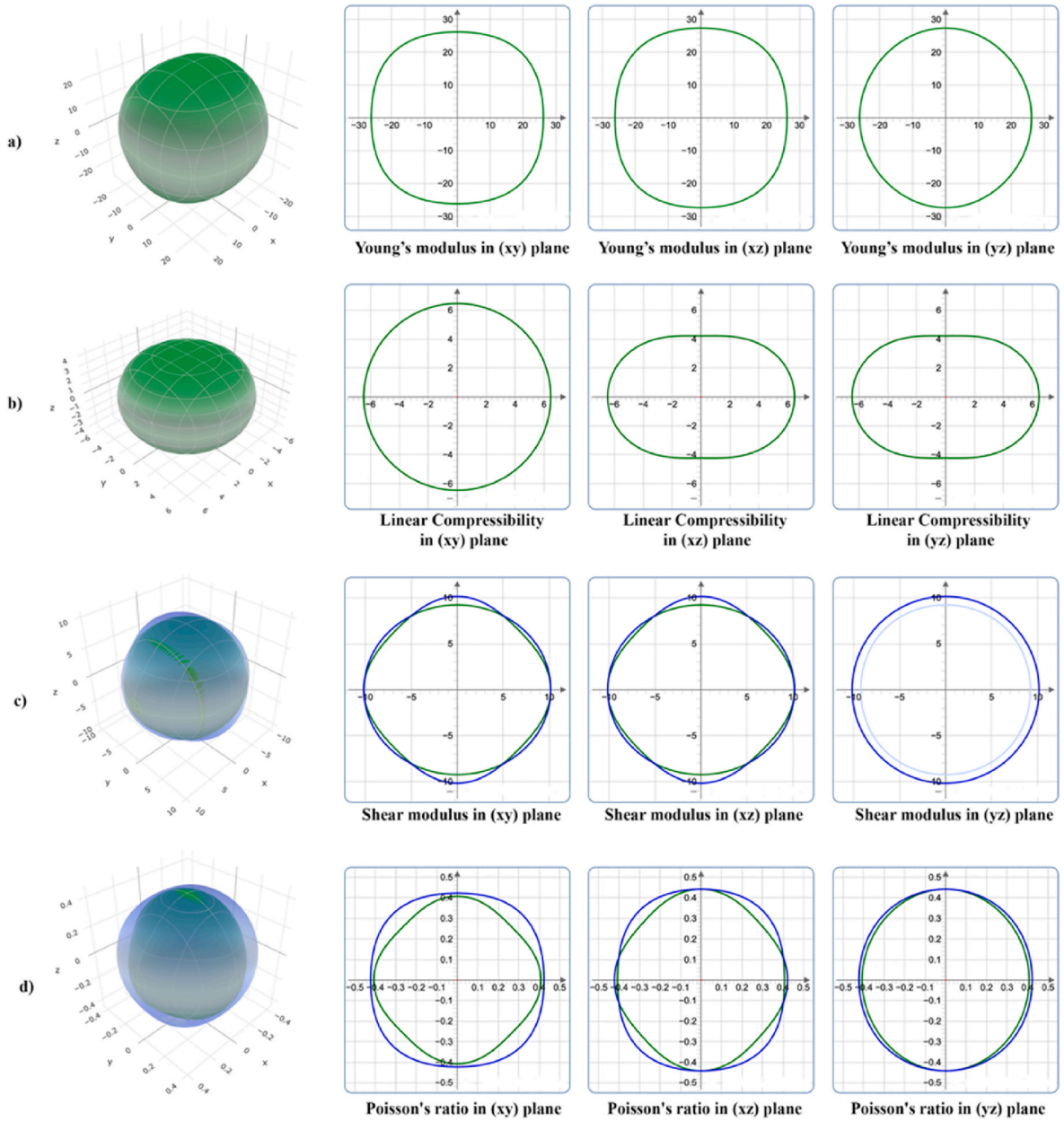

Fig. 7. The two- and three-dimensional (a) Young's modulus, (b) linear compressibility, (c) Shear modulus and (d) Poisson's ratio for $YMnS_2$.

$$v_t = \left(\frac{G}{\rho}\right)^{\frac{1}{2}} \tag{14}$$

$$v_m = \left[\frac{1}{3}\left(\frac{2}{v_t^3} + \frac{1}{v_l^3}\right)\right]^{-\frac{1}{3}} \tag{15}$$

4. Conclusion

$YMnS_2$ as a new ferromagnetic chalcopyrite belonging to I-42d space group with 122 space number has been investigated in this study. Negative formation energies prove that this chalcopyrite is energetically synthesizable and structurally stable. The plotted energy-volume curves and the calculated formation energies for three different types of magnetic phases show that the ferromagnetic phase is most stable for this compound.

The band gap values of $YMnS_2$ for spin-up orientation are calculated as 1.27 and 3.20 eV with PBE and HSE06 functionals, respectively. In addition, for spin-down orientation $YMnS_2$ is found to be in metallic nature with both functionals. Also, combination half metallic nature with 10^5 (cm^{-1}) order of absorption coefficient points out that $YMnS_2$ could be a good candidate for optoelectronic applications. Furthermore, $YMnS_2$ is mechanically stable due to satisfying the Born's stability criteria. Pugh's ratio around 6 for $YMnS_2$ indicates the ductile nature. Also, the value of Poisson's ratio around 0.422, means that the incompressibility of mentioned material is high and also it has ionic type atomic bonding. Shear anisotropy has been estimated for {001} and {100} planes and both estimated values indicated that $YMnS_2$ has anisotropic nature along these planes. It can be obviously understood from the visualized of some mechanical properties that Young's modulus, shear modulus and Poisson's ratio have isotropic nature in yz plane while linear compressibility has isotropic nature in (xy) plane. The present study shows that this material has very similar properties with the well-known chalcopyrite and lenaite compounds. However, there are no experimental and theoretical studies in the literature about this compound. As a conclusion, this computational study can help to better understand these types of materials and encourage related experimental works in future.

CRediT authorship contribution statement

Bugra Yildiz: Writing – original draft, Data curation, Visualization. **Aytac Erkisi:** Writing – review & editing, Formal analysis, Investigation. **Gokhan Surucu:** Conceptualization, Methodology, Investigation, Writing – review & editing.

Declaration of competing interest

The authors declare that they have no known competing financial interests or personal relationships that could have appeared to influence the work reported in this paper.

Acknowledgment

This research was supported in part by TÜBİTAK (The Scientific & Technological Research Council of Turkey) through TR-Grid e-Infrastructure Project, part of the calculations has been carried out at ULAKBİM Computer Center.

References

[1] N. Tsujii, T. Mori, High thermoelectric power factor in a carrier-doped magnetic semiconductor $CuFeS_2$, Appl. Phys. Express. 6 (2013), 043001, https://doi.org/10.7567/APEX.6.043001.

[2] R. Ang, A.U. Khan, N. Tsujii, K. Takai, R. Nakamura, T. Mori, Thermoelectricity generation and electron–magnon scattering in a natural chalcopyrite mineral from a deep-sea hydrothermal vent, Angew. Chem. Int. Ed. 54 (2015) 12909–12913, https://doi.org/10.1002/anie.201505517.

[3] F. Ahmed, N. Tsujii, T. Mori, Thermoelectric properties of $CuGa_{1-x}Mn_xTe_2$: power factor enhancement by incorporation of magnetic ions, J. Mater. Chem. A. 5 (2017) 7545–7554, https://doi.org/10.1039/C6TA11120C.

[4] L.I. Koroleva, D.M. Zashchirinskii, T.M. Khapaeva, A.I. Morozov, S.F. Marenkin, I. V. Fedorchenko, R. Szymczak, Manganese-doped $CdGeAs_2$, $ZnGeAs_2$ and $ZnSiAs_2$ chalcopyrites: a new materials for spintronics, J. Magn. Magn Mater. 323 (2011) 2923–2928, https://doi.org/10.1016/j.jmmm.2011.05.054.

[5] G.-B. Cha, W.S. Yun, S.C. Hong, Magnetocrystalline anisotropy of pure magnetic semiconductors of $MnGeP_2$ and $MnGeAs_2$: a first-principles study, J. Magn. Magn Mater. 419 (2016) 202–209, https://doi.org/10.1016/j.jmmm.2016.06.028.

[6] C. Tablero, Electronic and magnetic properties of the Fe-doped $CuInS_2$, Chem. Phys. Lett. 499 (2010) 75–78, https://doi.org/10.1016/j.cplett.2010.09.018.

[7] B. Djebour, H. Bouafia, B. Sahli, S. Hiadsi, B. Abidri, Structural, magnetic, and optoelectronic properties of CuMnSe2-chalcopyrite: DFT + U and hybrid functional investigation, J. Supercond. Nov. Magnetism 31 (2018) 1881–1893, https://doi.org/10.1007/s10948-017-4386-9.

[8] H. Bouhani-Benziane, O. Sahnoun, M. Sahnoun, M. Driz, C. Daul, Magnetic exchange interactions in Mn doped $ZnSnAs_2$ chalcopyrite, J. Magn. Magn Mater. 396 (2015) 345–349, https://doi.org/10.1016/j.jmmm.2015.08.025.

[9] R. Merikhi, B. Bennecer, A. Hamidani, Magneto-optical kerr effect in $ZnTMO_2$ (TM=Cr, Mn, Fe, Co and Ni), J. Magn. Magn Mater. 424 (2017) 327–338, https://doi.org/10.1016/j.jmmm.2016.10.089.

[10] M.N. Baibich, J.M. Broto, A. Fert, F.N. Van Dau, F. Petroff, P. Etienne, G. Creuzet, A. Friederich, J. Chazelas, Giant magnetoresistance of (001)Fe/(001)Cr magnetic superlattices, Phys. Rev. Lett. 61 (1988) 2472–2475, https://doi.org/10.1103/PhysRevLett.61.2472.

[11] I. Kars Durukan, Y. Oztekin Ciftci, First-principles calculations of vibrational and optical properties of half-Heusler NaScSi, Indian J. Phys. 95 (2021) 2303–2312, https://doi.org/10.1007/s12648-020-01887-0.

[12] C.I. Pearce, R.A.D. Pattrick, D.J. Vaughan, C.M.B. Henderson, G. van der Laan, Copper oxidation state in chalcopyrite: mixed Cu d9 and d10 characteristics, Geochem. Cosmochim. Acta 70 (2006) 4635–4642, https://doi.org/10.1016/j.gca.2006.05.017.

[13] I.M. Babar, S. Javaid, S. Rizvi, Transport properties of chalcopyrite ($CuFeS_2$) in a wide range of temperatures, J. Electron. Mater. 48 (2019) 2215–2218, https://doi.org/10.1007/s11664-019-06979-0.

[14] P. Baláž, E. Dutková, P. Levinský, N. Daneu, L. Kubíčková, K. Knížek, M. Baláž, J. Navrátil, J. Kašparová, V. Ksenofontov, A. Möller, J. Hejtmánek, Enhanced thermoelectric performance of chalcopyrite nanocomposite via co-milling of synthetic and natural minerals, Mater. Lett. 275 (2020) 128107, https://doi.org/10.1016/j.matlet.2020.128107.

[15] S. Conejeros, P. Alemany, M. Llunell, I. de P.R. Moreira, V. Sánchez, J. Llanos, Electronic structure and magnetic properties of $CuFeS_2$, Inorg. Chem. 54 (2015) 4840–4849, https://doi.org/10.1021/acs.inorgchem.5b00399.

[16] R. Khaledialidusti, A.K. Mishra, A. Barnoush, Temperature-dependent properties of magnetic $CuFeS_2$ from first-principles calculations: structure, mechanics, and thermodynamics, AIP Adv 9 (2019), 065021, https://doi.org/10.1063/1.5084308.

[17] Z. Wei, Y. Li, H. Gao, Y. Zhu, G. Qian, J. Yao, New insights into the surface relaxation and oxidation of chalcopyrite exposed to O_2 and H_2O: a first-principles DFT study, Appl. Surf. Sci. 492 (2019) 89–98, https://doi.org/10.1016/j.apsusc.2019.06.191.

[18] H. Takaki, K. Kobayashi, M. Shimono, N. Kobayashi, K. Hirose, N. Tsujii, T. Mori, First-principles calculations of Seebeck coefficients in a magnetic semiconductor $CuFeS_2$, Appl. Phys. Lett. 110 (2017), 072107, https://doi.org/10.1063/1.4976574.

[19] J. Park, Y. Xia, V. Ozoliņš, First-principles assessment of thermoelectric properties of $CuFeS_2$, J. Appl. Phys. 125 (2019) 125102, https://doi.org/10.1063/1.5088165.

[20] S. Conejeros, P. Alemany, M. Llunell, I. de P.R. Moreira, V. Sánchez, J. Llanos, Electronic structure and magnetic properties of $CuFeS_2$, Inorg. Chem. 54 (2015) 4840–4849, https://doi.org/10.1021/acs.inorgchem.5b00399.

[21] D. Huertas-Hernando, F. Guinea, A. Brataas, Spin-orbit coupling in curved graphene, fullerenes, nanotubes, and nanotube caps, Phys. Rev. B 74 (2006) 155426, https://doi.org/10.1103/PhysRevB.74.155426.

[22] D. Vijayalakshmi, G. Kalpana, Electronic structure and magnetic properties of chalcopyrite type $ZnMX_2$ (M = Sc, V, Cr, Mn, Fe; X = P, As) compounds: an ab initio study, Phys. Status Solidi 253 (2016) 1576–1584, https://doi.org/10.1002/pssb.201552554.

[23] J.W. Boon, The crystal structure of $NaBiS_2$ and $KBiS_2$, Recl. Des Trav. Chim. Des Pays-Bas. 63 (2010) 32–34, https://doi.org/10.1002/recl.19440630203.

[24] V. Kumar, B.S.R. Sastry, Heat of formation of ternary chalcopyrite semiconductors, J. Phys. Chem. Solid. 66 (2005) 99–102, https://doi.org/10.1016/j.jpcs.2004.08.034.

[25] T. Djaafri, H. Bouafia, B. Sahli, B. Djebour, Ş. Uğur, G. Uğur, H. Moussa, Study of the ground-state magnetic ordering, magnetic and optoelectronic properties of (Lenaite) $AgFeS_2$ in its chalcopyrite structure, J. Magn. Magn Mater. 493 (2020) 165730, https://doi.org/10.1016/j.jmmm.2019.165730.

[26] X. Yu, Z. Zhang, J. Xie, Effects of rare earth elements doping on ordered structures and ductility improvement of Fe–6.5wt%Si alloy, Mater. Lett. 184 (2016) 294–297, https://doi.org/10.1016/j.matlet.2016.08.074.

[27] J. Mercier, G. Zambelli, G. Kurz, Introduction to Materials Science, Éditions Sci. Medicales Elsevier SAS, 2002.

[28] P.E. Blöchl, Projector augmented-wave method, Phys. Rev. B 50 (1994) 17953–17979, https://doi.org/10.1103/PhysRevB.50.17953.

[29] W. Kohn, L.J. Sham, Self-consistent equations including exchange and correlation effects, Phys. Rev. 140 (1965) A1133–A1138, https://doi.org/10.1103/PhysRev.140.A1133.

[30] P. Hohenberg, W. Kohn, Inhomogeneous electron gas, Phys. Rev. 136 (1964) B864–B871, https://doi.org/10.1103/PhysRev.136.B864.
[31] J.P. Perdew, K. Burke, M. Ernzerhof, Generalized gradient approximation made simple, Phys. Rev. Lett. 77 (1996) 3865–3868, https://doi.org/10.1103/PhysRevLett.77.3865.
[32] H.J. Monkhorst, J.D. Pack, Special points for Brillouin-zone integrations, Phys. Rev. B 13 (1976) 5188–5192, https://doi.org/10.1103/PhysRevB.13.5188.
[33] J. Heyd, G.E. Scuseria, M. Ernzerhof, Hybrid functionals based on a screened Coulomb potential, J. Chem. Phys. 118 (2003) 8207–8215, https://doi.org/10.1063/1.1564060.
[34] A.V. Krukau, O.A. Vydrov, A.F. Izmaylov, G.E. Scuseria, Influence of the exchange screening parameter on the performance of screened hybrid functionals, J. Chem. Phys. 125 (2006) 224106, https://doi.org/10.1063/1.2404663.
[35] Y. Le Page, P. Saxe, Symmetry-general least-squares extraction of elastic coefficients from ab initio total energy calculations, Phys. Rev. B 63 (2001) 174103, https://doi.org/10.1103/PhysRevB.63.174103.
[36] R. Gaillac, P. Pullumbi, F.-X. Coudert, ELATE: an open-source online application for analysis and visualization of elastic tensors, J. Phys. Condens. Matter 28 (2016) 275201, https://doi.org/10.1088/0953-8984/28/27/275201.
[37] S.W. Lovesey, K.S. Knight, C. Detlefs, S.W. Huang, V. Scagnoli, U. Staub, Acentric magnetic and optical properties of chalcopyrite ($CuFeS_2$), J. Phys. Condens. Matter 24 (2012) 216001, https://doi.org/10.1088/0953-8984/24/21/216001.
[38] T.W.G. Wyckoff, Crystal Structures -, New York Intersci. Publ., 1963.
[39] G. Surucu, A. Gencer, X. Wang, O. Surucu, Lattice dynamical and thermo-elastic properties of M_2AlB (M = V, Nb, Ta) MAX phase borides, J. Alloys Compd. 819 (2020) 153256, https://doi.org/10.1016/j.jallcom.2019.153256.
[40] T. Yang, L. Jin, Y. Liu, X. Zhang, X. Wang, Spin-polarized type-II nodal loop and nodal surface states in hexagonal compounds $XTiO_2$= Li, Na, K, Rb), Phys. Rev. B 103 (2021) 235140, https://doi.org/10.1103/PhysRevB.103.235140.
[41] P. Vinet, J.H. Rose, J. Ferrante, J.R. Smith, Universal features of the equation of state of solids, J. Phys. Condens. Matter 1 (1989) 1941–1963, https://doi.org/10.1088/0953-8984/1/11/002.
[42] S.R. Hall, J.M. Stewart, The crystal structure refinement of chalcopyrite, $CuFeS_2$, Acta Crystallogr. Sect. B Struct. Crystallogr. Cryst. Chem. 29 (1973) 579–585, https://doi.org/10.1107/S0567740873002943.
[43] W. Tang, E. Sanville, G. Henkelman, A grid-based Bader analysis algorithm without lattice bias, J. Phys. Condens. Matter 21 (2009), 084204, https://doi.org/10.1088/0953-8984/21/8/084204.
[44] M.V. Lalić, Z.S. Popović, F.R. Vukajlović, Ab initio study of electronic, magnetic and optical properties of $CuWO_4$ tungstate, Comput. Mater. Sci. 50 (2011) 1179–1186, https://doi.org/10.1016/j.commatsci.2010.11.018.
[45] N.V. Smith, Photoelectron energy spectra and the band structures of the noble metals, Phys. Rev. B 3 (1971) 1862–1878, https://doi.org/10.1103/PhysRevB.3.1862.
[46] A. Erkişi, G. Gökoğlu, G. Sürücü, R. Ellialtıoğlu, E.K. Yıldırım, First-principles investigation of $LaGaO_3$ and $LaInO_3$ lanthanum perovskite oxides, Philos. Mag. 96 (2016) 2040–2058, https://doi.org/10.1080/14786435.2016.1189100.
[47] C. Ambrosch-Draxl, J.O. Sofo, Linear optical properties of solids within the full-potential linearized augmented planewave method, Comput. Phys. Commun. 175 (2006) 1–14, https://doi.org/10.1016/j.cpc.2006.03.005.
[48] S. Malki, L. El Farh, Ab initio study of optoelectronic properties of VSb_2 compound, Int. J. Nanoelectron. Mater. 13 (2020) 591–600.
[49] A. Gencer, Electronic and optical properties of ASc_2S_4 (A = Ca, Sr) compounds, Phys. Scripta 96 (2021), 075805, https://doi.org/10.1088/1402-4896/abf796.
[50] A. Gencer, O. Surucu, G. Surucu, E. Deligoz, Anisotropic mechanical properties of $Tl_4Ag_{18}Te_{11}$ compound with low thermal conductivity, J. Solid State Chem. 289 (2020) 121469, https://doi.org/10.1016/j.jssc.2020.121469.
[51] C. Li, B. Wang, R. Wang, H. Wang, X. Lu, First-principles study of structural, elastic, electronic, and optical properties of orthorhombic $BiGaO_3$, Comput. Mater. Sci. 42 (2008) 614–618, https://doi.org/10.1016/j.commatsci.2007.09.008.
[52] A. Reuss, Berechnung der Fließgrenze von Mischkristallen auf Grund der Plastizitätsbedingung für Einkristalle, ZAMM - Zeitschrift Für Angew. Math. Und Mech. 9 (1929) 49–58, https://doi.org/10.1002/zamm.19290090104.
[53] W. Voigt, Lehrbuch der kristallphysik (mit ausschluss der kristalloptik), 1928. Leipzig, Berlin, B.G. Teubner.
[54] R. Hill, The elastic behaviour of a crystalline aggregate, Proc. Phys. Soc. 65 (1952) 349–354, https://doi.org/10.1088/0370-1298/65/5/307.
[55] G. Surucu, B. Yildiz, A. Erkisi, X. Wang, O. Surucu, The investigation of electronic, anisotropic elastic and lattice dynamical properties of MAB phase nanolaminated ternary borides: M_2AlB_2 (M=Mn, Fe and Co) under spin effects, J. Alloys Compd. 838 (2020) 155436, https://doi.org/10.1016/j.jallcom.2020.155436.
[56] S.F. Pugh, XCII. Relations between the elastic moduli and the plastic properties of polycrystalline pure metals, London, Edinburgh, Dublin Philos. Mag. J. Sci. 45 (1954) 823–843, https://doi.org/10.1080/14786440808520496.
[57] A. Erkisi, G. Surucu, The electronic and elasticity properties of new half-metallic chalcogenides Cu_3TMCh_4 (TM = Cr, Fe and Ch = S, Se, Te): an ab initio study, Philos. Mag. 99 (2019) 513–529, https://doi.org/10.1080/14786435.2018.1546960.
[58] V.V. Bannikov, I.R. Shein, A.L. Ivanovskii, Electronic structure, chemical bonding and elastic properties of the first thorium-containing nitride perovskite $TaThN_3$, Phys. Status Solidi Rapid Res. Lett. 1 (2007) 89–91, https://doi.org/10.1002/pssr.200600116.
[59] P. Ravindran, L. Fast, P.A. Korzhavyi, B. Johansson, J. Wills, O. Eriksson, Density functional theory for calculation of elastic properties of orthorhombic crystals: application to $TiSi_2$, J. Appl. Phys. 84 (1998) 4891–4904, https://doi.org/10.1063/1.368733.
[60] E. Schreiber, O.L. Anderson, S. Naohiro, Elastic Constants and Their Measurement, McGraw-Hill, New York, 1973.
[61] D.G. Cahill, S.K. Watson, R.O. Pohl, Lower limit to the thermal conductivity of disordered crystals, Phys. Rev. B 46 (1992) 6131–6140, https://doi.org/10.1103/PhysRevB.46.6131.
[62] D.R. Clarke, C.G. Levi, Materials design for the next generation thermal barrier coatings, Annu. Rev. Mater. Res. 33 (2003) 383–417, https://doi.org/10.1146/annurev.matsci.33.011403.113718.
[63] J. Wu, X. Wei, N.P. Padture, P.G. Klemens, M. Gell, E. García, P. Miranzo, M. I. Osendi, Low-thermal-conductivity rare-earth zirconates for potential thermal-barrier-coating applications, J. Am. Ceram. Soc. 85 (2004) 3031–3035, https://doi.org/10.1111/j.1151-2916.2002.tb00574.x.